WELDING RESEARCH

SUPPLEMENT TO THE *WELDING JOURNAL*, JULY 1994
Sponsored by the American Welding Society and the Welding Research Council

RESEARCH/DEVELOPMENT/RESEARCH/DEVELOPMENT/RESEARCH/DEVELOPMENT/RESEARCH/DEVELOPMENT

Wettability of Metallic Glass Alloys by Two Tin-Based Solders

The feasibility of using soldering as a joining technique for metallic glasses is examined

BY P. T. VIANCO, F. M. HOSKING AND J. A. REJENT

ABSTRACT. The wettability of 95Sn-5Sb (wt-%) and 96.5Sn-3.5Ag solder alloys on rapidly solidified metal ribbons of compositions: 92Fe-3B-5Si, 81Co-4Fe-1Ni-4Mo-3B-7Si, and 82Co-5Fe-1Ni-3B-9Si was analyzed by the meniscometer/wetting balance technique. Two organic acid fluxes and an inorganic acid flux were evaluated. The substrate surfaces received only a solvent degreasing treatment. The 96.5Sn-3.5Ag and 95Sn-5Sb solders exhibited fair to good wetting with contact angles of 32 to 62 deg and 25 to 60 deg, respectively. The contact angle values were similar with the two organic acid fluxes and slightly lower with the inorganic acid solution. Although the surface morphology was different on the two faces of the ribbons, the contact angles of either surface for each ribbon were similar. The quality of the solder film remaining on the samples was largely dependent upon the particular solder-flux-substrate system with the exception of the inorganic flux for which dewetting was always observed. The solder-flux interfacial tension values depended upon the flux and solder alloy. Thermal annealing of the metallic glass caused a deterioration in wettability. Undetected changes to the thickness of the native surface oxide layer, or the thermally relaxed structure resulting from the heat treatment, were likely sources of the increased contact angle.

P. T. VIANCO, F. M. HOSKING and J. A. REJENT are with the Center for Solder Science and Technology, Sandia National Laboratories, Albuquerque, N.Mex.

KEY WORDS

Soldering
Tin-Based Solders
Wettability
Metallic Glass Alloy
Structural Relaxation
Organic Acid Flux
Inorganic Acid Flux
Contact Angle
Morphology
Surface Cleaning

Introduction

Metallic Glasses

Rapidly solidified amorphous metals (or metallic glasses) have demonstrated commercial success in the fabrication of low loss transformer cores and magnetic shielding components (Refs. 1, 2). The variety of metal compositions available for fabrication has been largely responsible for the range of applications. The use of these materials will grow as other properties such as excellent wear and corrosion resistance become fully realized.

Metallic glass ribbons are fabricated by depositing a stream of molten alloy onto a rapidly spinning wheel — Fig. 1A. The wheel quenches the metal at rates approaching 10^{6}°C/s. The individual atoms are literally frozen into a random arrangement characteristic of the liquid state. This is compared to the long-range order of the crystalline state (Fig. 1B), which characterizes most metal alloys. The typical shape of the solidified metallic glass is that of a foil with dimensions 0.0025 cm (0.001 in.) thick and widths in the range of 0.3 to 15 cm (0.12 to 6 in.). The thickness of the ribbon is limited to less than 0.01 cm (0.004 in.); otherwise, the molten stream is not solidified rapidly enough to retain the amorphous structure.

The amorphous structure of these materials is metastable; that is, under the application of heat, the atoms will rearrange themselves so as to increase the short range order within the structure, but still retain the amorphous state. This process is termed "structural relaxation." If the temperature is great enough, however, the atoms will further change their configuration so as to finally develop the long-range order of the crystalline state — Fig. 1B. The atomic rearrangements which comprise structural relaxation and crystallization cause changes to the mechanical, physical, and electromagnetic properties of these materials.

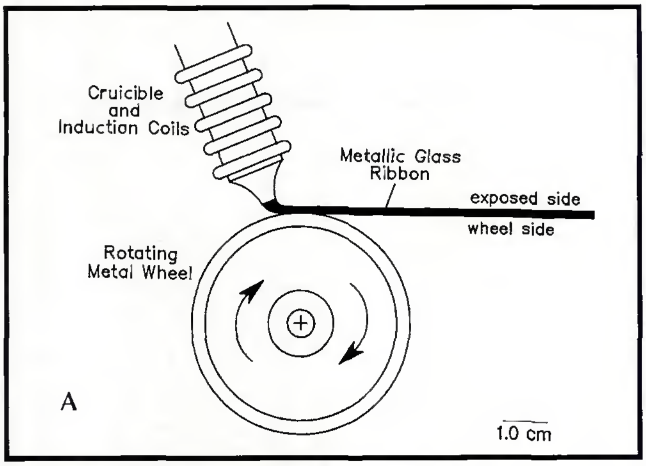

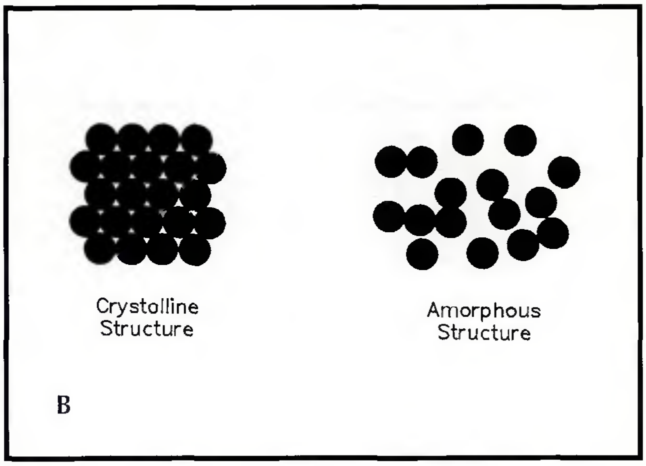

Fig. 1 — A — Melt spinning technique used to fabricate the metallic glass ribbons; B — schematic diagram of the atomic arrangements in the amorphous and crystalline solid states.

One consideration for the introduction of metallic glasses into engineered assemblies is joining. Aside from mechanical fastening techniques, candidate processes are limited to those involving relatively low temperatures due to the thermal instability of the amorphous structure. Therefore, a study was initiated to examine soldering as a joining technique for metallic glasses. The first goal of this investigation was to establish the solderability of metallic glasses as a function of solder alloy, flux, and surface preparation procedures. The second goal was to examine the effect of structural relaxation on the wetting properties; this phenomena was of interest from the viewpoint of surface science as well as from a more practical standpoint. Numerous engineering properties of metallic glasses (*e.g.*, magnetic susceptibility and hardness) are optimized by specific thermal annealing treatments prior to their use.

Analysis of Wettability

Calculating the Wettability Parameters

The wettability of solder alloys on metallic glass substrates was quantitatively assessed by measurements of the contact angle, θ_c, formed at the solder-substrate-flux triple point of a substrate coupon immersed edge-on into a bath of molten solder — Fig. 2. The contact angle is determined by the equilibrium balance of the three interfacial tensions: substrate (S)-flux (F), γ_{SF}; substrate (S)-molten solder (L), γ_{SL}; and molten solder (L)-flux (F), γ_{LF}; through Young's equation shown at the bottom of the figure. A consequence of the process used to fabricate the ribbons is that the surface which contacted the copper wheel ("wheel side") exhibits a surface morphology which is different from that of the "exposed side." The differences may be strictly in the physical topology, as illustrated in Fig. 3, or include atomic structure variations such as degrees of short range order or chemical segregation. Both surfaces possessed striations in the casting direction; the scale of these features was much finer

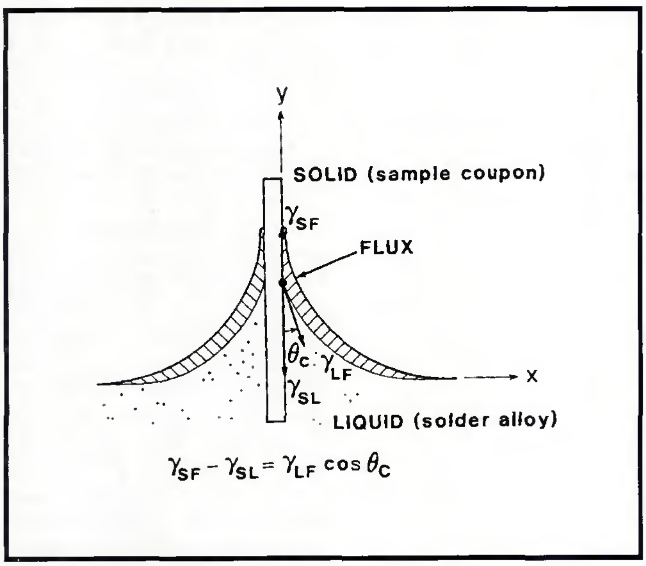

Fig. 2 —Schematic diagram of the equilibrium geometry between the interfacial tensions and the contact angle at the solder-substrate-flux triple point. Below the figure is Young's equation.

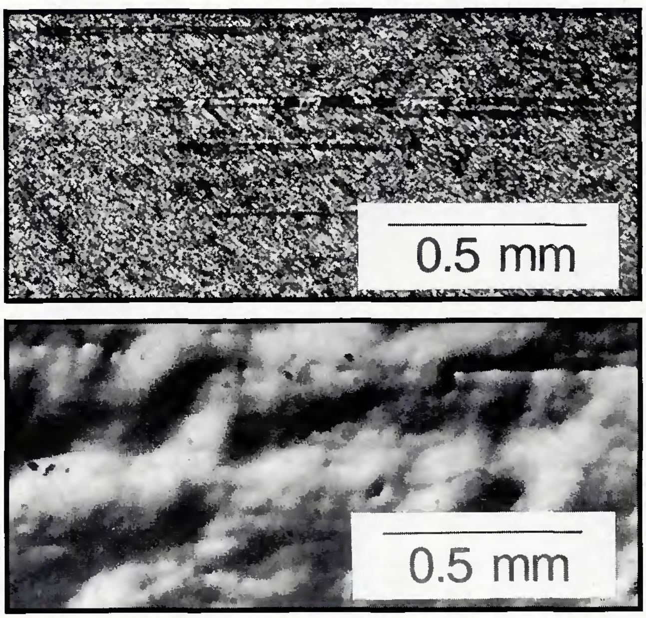

Fig. 3 — Optical micrographs of a sample of the 2705M cobalt-based metallic glass ribbon. Top — Wheel side; Bottom — exposed side.

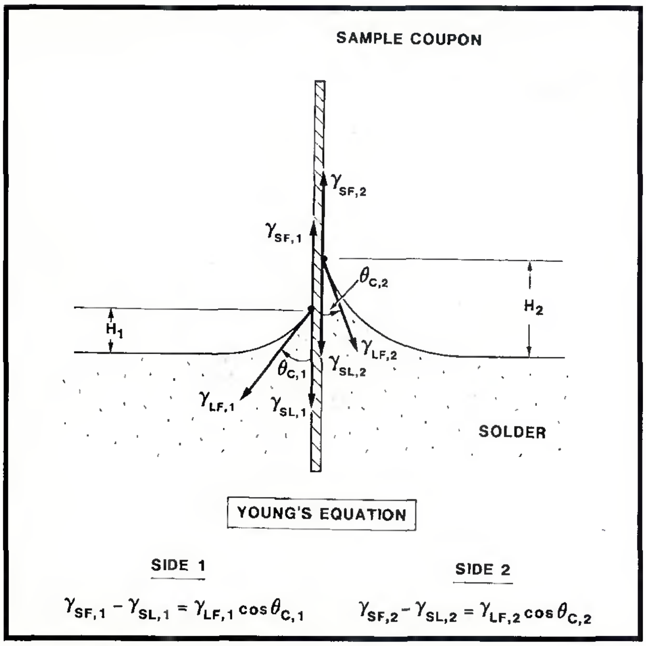

Fig. 4 — Schematic diagram of wetting with nonsymmetric meniscus heights.

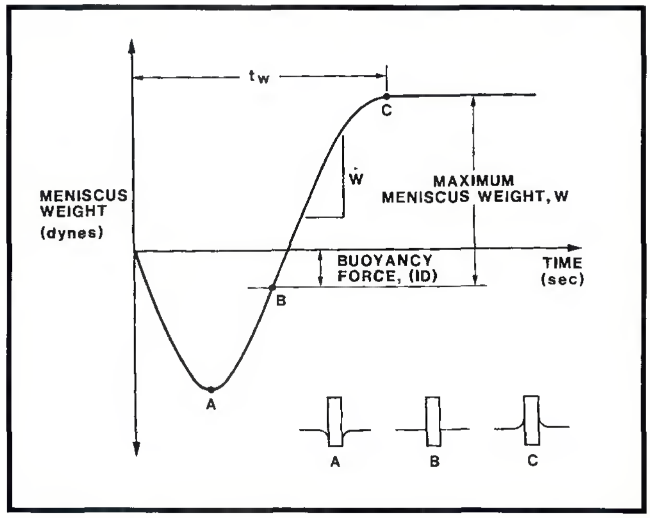

Fig. 5 — Typical wetting curve of meniscus weight as a function of time, depicting the manner in which the wetting rate and wetting time are identified.

on the wheel side than the exposed side of the foils. It was conceivable that the solder meniscus would not rise equally on both sides of the ribbon — Fig 4. Nevertheless, Young's equation would apply to either face of the coupon.

Analytical expressions were developed which would calculate the contact angles, $\theta_{c,1}$, and, $\theta_{c,2}$, from the three experimentally measured parameters: H_1, H_2, and the combined weight of the two menisci, W. A derivation of the analytical expression required the assumption that the solder-flux interfacial tension, γ_{LF}, be the same around the entire sample perimeter. The factors which influence the value of γ_{LF} are 1) the solder composition, 2) the type of flux coating, and to a lesser extent, 3) the by-products generated by the fluxing action. Since the same flux and solder is present on the two sides of the coupon, only point three needed to be considered for the validity of the assumption. Visual examination of the flux film on the sample was made prior to immersion and after completion of the test. No differences in the color or clarity of the coatings on either side of the specimens, were observed. Therefore, it was assumed that γ_{LF} was similar on both surfaces of a particular sample.

The expressions for the contact angles will now be developed. First, the cross-sectional area of the meniscus on either side of the sample is given by (Ref. 3):

$$A_i = \frac{H_i}{2}\sqrt{\frac{4\gamma_{LF}}{\rho g} - H_i^2} \tag{1}$$

where i=1, 2 designates the two sample faces. The symbol, ρ, is the solder density and g is the acceleration due to gravity. The weight of each meniscus is determined by multiplying A_i by $\rho g(P/2)$ where P is the sample perimeter. The solder meniscus along the sample thickness was assumed to exhibit an "average" behavior between those on the two broad faces. The total weight of the meniscus on the immersed sample, W, is given by:

$$W = \frac{\rho g P}{4}\left(H_1\sqrt{\frac{4\gamma_{LF}}{\rho g} - H_1^2} + H_2\sqrt{\frac{4\gamma_{LF}}{\rho g} - H_2^2} \right) \tag{2}$$

Equation 2 is solved transcendentally for the value of γ_{LF}. This parameter was then used to calculate the contact angles, $\theta_{c,1}$ and $\theta_{c,2}$ from the following expression (Ref. 4):

$$\theta_{c,\,i} = \sin^{-1}\left(1 - \frac{\rho g H_i^2}{2\gamma_{LF}}\right) \tag{3}$$

Finally, the wetting curves of meniscus weight vs. time were analyzed to determine the value of t_W, the time to reach the maximum meniscus weight and $\dot{W}$, the rate of meniscus rise on the coupon. These two parameters are measured as illustrated on the exemplary wetting curve in Fig. 5. The wetting rate measurements cannot distinguish the rates of meniscus rise on either of the two ribbon surfaces. Therefore, this data represent an average measurement and were used only for relative comparisons between the sample sets.

Tilt of the Sample Caused by the Nonsymmetric Meniscus Rise

The different meniscus dimensions shown in Fig. 4 place a torque on the sample, causing it to tilt from the vertical plane. The rotation causes the true contact angles to be different from the "apparent" values calculated with H_1, H_2, and W using Equation 3. The magnitude of the rotation depends upon the centroid coordinates and the weight of the two menisci. An analysis was performed which generated the equations for the meniscus centroid coordinates. These expressions were then used to derive the tilt angle of a coupon caused by the nonsymmetric meniscus rise. A summary of those computations appears below.

The calculation of the tilt angle begins with determining the expressions for the x and y coordinates of the centroid of the meniscus profile (see Fig. 1 for the orientation of the x and y axes). The equation for the x coordinate of the centroid, $\bar{x}_i$, as measured from x = 0 at the coupon surface, is given as (Ref. 5):

$$\bar{x}_i = \frac{1}{A_i}\int x\,dA \tag{4}$$

where A_i is the cross-sectional area of the meniscus as given in Equation 1. The meniscus profile is described by the function x(y) (Ref. 4):

$$x(y)=\frac{1}{2\sqrt{k}}\left\{\begin{array}{l}\frac{1}{2\sqrt{2}}\ln\left[\frac{1+\sqrt{\left(1-ky^2\right)}}{1-\sqrt{\left(1-ky^2\right)}}\right]- \\ \frac{1}{2\sqrt{2}}\ln\left[\frac{1+\sqrt{\left(1-kH^2\right)}}{1-\sqrt{\left(1-kH^2\right)}}\right]- \\ \sqrt{2}\sqrt{\left(1-ky^2\right)}+ \\ \sqrt{2}\sqrt{\left(1-kH^2\right)}\end{array}\right\} \quad (5)$$

where k is the constant, $(\rho g)/4\gamma_{LF}$. The expression for the differential area, dA, is given as x(y)dy. Therefore, the equation to determine $\bar{x}_i$ is:

$$\bar{x}_i=\frac{1}{2A_i}\int_0^{H_i}\left[x(y)\right]^2 dy \quad (6)$$

The expression for the x coordinate of the centroid is:

$$\bar{x}_i=\frac{H_i}{4kA_i}\left(1-\frac{2}{3}kH_i^{\ 2}\right) \quad (7)$$

The y coordinate of the solder meniscus centroid, $\bar{y}_i$, measured from y = 0 as defined by the undisturbed solder level, is determined by the equation:

$$\bar{y}_i=\frac{1}{A_i}\int_0^{H_i} y\left[x(y)\right] dy \quad (8)$$

where A_i is described by Equation 1. The expression for y_i is given as:

$$\bar{y}_i=\frac{1}{3kH_i}\left[kH_i^2-\frac{1}{2\sqrt{\left(1-kH_i^2\right)}}+\frac{1}{2}\right] \quad (9)$$

Listed in Table 1 are values for $\bar{x}$ and $\bar{y}$ determined from values of ρ, H, and γ_{LF} which are commonly observed in engineering solder systems. The first two sets of data clearly show that increasing the value of H_i decreases $\bar{x}$ and increases $\bar{y}$; the change is smaller for $\bar{x}$ relative to $\bar{y}$. The roles of solder density and interfacial tension are illustrated in the accompanying data sets.

The weight of each meniscus, W_i, which is located at the centroid coordinates, $(\bar{x}_i, \bar{y}_i)$, generates a torque on the sample. The tilt angle of the coupon from the vertical plane, δ, is determined by the equilibrium balance between the torques from the two menisci. A schematic diagram of the load-moment arm geometry is illustrated in Fig. 6. In the derivation of the expression for δ, it was assumed that 1) the tilt angle was small so that changes in the centroid location were negligible, and 2) the sample rotated as a rigid structure about the hinge point. Both assumptions will cause a small overestimation of the tilt angle. A more precise computation would necessarily involve an analysis of the mechanics of large deflections in thin plates.

Several trigonometric manipulations result in the following expression for the tilt angle, δ:

$$\delta=\tan^{-1}\left[\frac{W_2\bar{x}_2-W_1\bar{x}_1}{\left(L_3-ID\right)\left(W_1+W_2\right)-W_1\bar{y}_1-W_2\bar{y}_2}\right] \quad (10)$$

The parameter, L_3, represents the distance from the "hinge point" to the bottom of the coupon (Fig. 6), and ID is the immersion depth. Shortening the value of L_3 increases the value of δ.

Shown in Table 2 are values of the tilt angle as a function of typical solder densities, solder-flux interfacial tensions, and

Table 1 — Coordinates of the Meniscus Center of Gravity as a Function of Typical Solder Density, Interfacial Tension, and Meniscus Height Values

Solder Density (g/cm^3)	Solder-Flux Interfacial Tension (dyne/cm)	Meniscus Height (cm)	$\bar{X}$ (cm)	$\bar{y}$ (cm)
7.28	400	0.170	0.232	0.0410
7.28	400	0.230	0.228	0.0533
7.28	700	0.170	0.309	0.0417
8.49	400	0.230	0.210	0.0523
8.49	700	0.230	0.283	0.0549

Table 2 — Effect of Typical Solder Properties on the Sample Tilt for a Nonsymmetric Meniscus Rise (L_3 = 2.54 cm)

Solder Density (g/cm^3)	γ_{LF} (dyne/cm)	H_1 (cm)	H_2 (cm)	$\lvert H_1-H_2\rvert$ (cm)	Tilt Angle (deg)
7.28	400	0.170	0.230	0.050	0.693
7.28	700	0.170	0.230	0.050	1.084
8.49	400	0.170	0.230	0.050	0.594
8.49	700	0.170	0.230	0.050	0.971

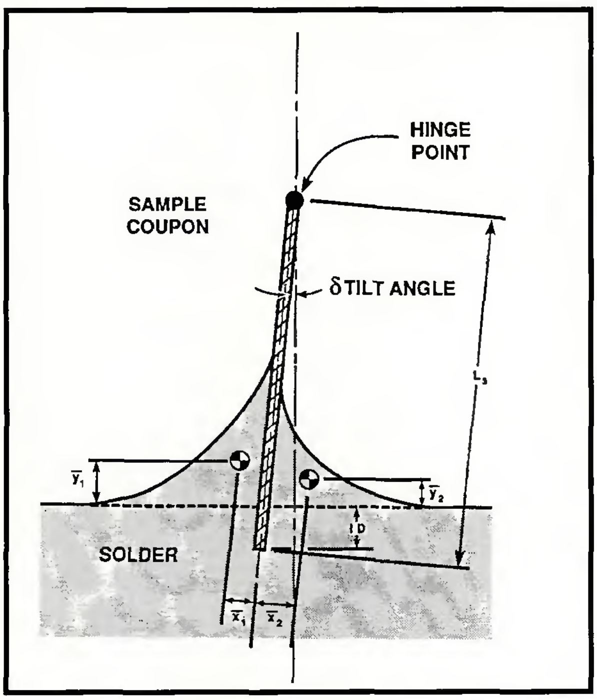

Fig. 6 — Schematic diagram of the load-moment geometry caused by the nonsymmetric meniscus rise.

Table 3 — Chemical Composition and Crystallization Temperature of the Metallic Glass Alloys

Metallic Glass Alloy	Nominal Composition (wt/%)	Crystallization Temperature (C)
2605S-2	92Fe-3B-5Si	550
2705M	81Co-4Fe-1 Ni-4Mo-3B-7Si	520
2714A	82Co-5Fe-1 Ni-3B-9Si	550

Table 4 — Meniscus Height as a Function of Sample Orientation Relative to the Immersion Direction

	Meniscus Height and Sample Orientation			
	Vertical		Horizontal	
Alloy, Solder, Flux	H (exposed) (cm)	H (wheel) (cm)	H (exposed) (cm)	H (wheel) (cm)
2714A 96.5Sn-3.5Ag A260HF	0.248 ± 0.009	0.248 ± 0.009	0.202 ± 0.005	0.262 ± 0.008
2705M 95Sn-5Sb A260HF	0.197 ± 0.006	0.217 ± 0.010	0.161 ± 0.004	0.236 ± 0.006
2605S-2 95Sn-5Sb A260HF	0.159 ± 0.016	0.137 ± 0.010	0.137 ± 0.014	0.155 ± 0.010

the meniscus heights. The values of H_1, H_2, γ_{LF}, and ρ represent the range anticipated for this study. The value of L_3 was 2.54 cm (1 in.). The maximum value of δ was 1.08 deg, which is well within the experimental error of testing apparatus (±1.3 deg). Therefore, although the wetting performance anticipated from the tests in this study was not expected to differ significantly from those used to calculated the values in Table 2, computations were performed with actual experimental data to confirm this assumption.

Experimental

The metallic glasses examined in this study were taken from commercial product made by Metglas™ Div., Allied Signal Corp. The alloys were those designated as (1) 2605S-2, (2) 2714A, and (3) 2705M. The nominal compositions and crystallization temperatures of the alloys are listed in Table 3. These particular alloys were selected in order to evaluate wetting on both iron- and cobalt-based amorphous materials. The two cobalt-based substrates were chosen in order to examine whether differences in alloy composition affect the wetting behavior. The sample coupons, which measured 0.0025 ±0.0002 x 2.54 ±0.002 x 2.54 ±0.002 cm, were cleaned by degreasing for 5 min in a trichloroethylene ultrasonic rinse (25°C; 77°F), followed by a 2 min. rinse in isopropyl alcohol (25°C). The samples were then dried in a stream of N_2 gas after which they were immediately coated with the appropriate flux.

The two solders tested were 96.5Sn-3.5Ag (wt-%) with a eutectic temperature of 221°C (430°F), and 95Sn-5Sb having a liquidus temperature of 240°C (464°F) and a solidus temperature of 232°C (450°F). Each solder was used at a temperature of 267° ±1°C.

The fluxes used to coat the coupons included: 1) Alpha™260HF (abbreviated A260HF) (Ref. 6), an alcohol-based, organic acid; 2) Blackstone™1452 (B1452) (Ref. 7), a water-based, organic acid; and 3) Alpha™200L (A200L), an inorganic acid[1]. Each of the fluxes was used at full strength.

The experimental tests were comprised of measuring: 1) the meniscus heights on the two faces of the coupons and 2) the total weight of the solder meniscus. The methodology for analyzing a homogeneous sample is described in Ref. 3. The samples were immersed into the solder pots with the casting direction parallel to the immersion direction. The meniscus heights were determined with a meniscometer, which is a precision traveling microscope. The meniscus weight data were acquired by the wetting balance technique. The wetting balance apparatus used a computer-controlled stepper motor to raise the solder pot at a rate of 1.3 cm/s (3.3 in./s) until the sample had been immersed to 0.4 cm (0.16 in.). The samples were then automatically withdrawn after 20 s. The data, which are described by meniscus weight vs. time (Fig. 5), were stored in a microcomputer. The maximum meniscus weight, W, was determined from each of these curves. A total of 10 samples was used in the meniscometer tests, five each to determine the menisci heights on the two surfaces of the coupon (H_1 and H_2). The meniscus weight was the average of data taken from six coupons. The parameters, γ_{LF}, $\theta_{c,1}$, and $\theta_{c,2}$, were determined from the mean values of H_1, H_2, and W using Equations 2 and 3. An error interval was developed for the contact angles and interfacial tension as follows: A maximum-minimum value range was defined for each of H_1, H_2, and W as plus-or-minus one standard deviation about the respective means. The maximum and minimum values of H_1, H_2, and W were then introduced into Equations 2 and 3 in combinations that gave the maximum and minimum values of γ_{LF}, $\theta_{c,1}$, and $\theta_{c,2}$ which defined the (±) error terms for the mean values.

1. No endorsement is made for the use of these commercial products. Their selection was based upon their different activities relative to the more common rosin-based fluxes.

Results and Discussion

Dependence of Meniscus Height on Sample Orientation

The effect of the orientation of the surface features was investigated by measuring the solder meniscus height on both sides of samples with the casting direction oriented either vertically or horizontally with respect to the immersion direction. Each of the three alloys was tested with the same flux, A260HF, and either one of the two solders. The results are summarized in Table 4. The two cobalt-based alloys exhibited a significant decrease and increase of the exposed and wheel side meniscus heights, respectively, going from the vertical to the horizontal orientation. For these two metallic glass alloys, the change was approximately 18 to 19% for the exposed surface and 5 to 8% on the wheel side. A similar trend was observed in the mean values of the meniscus heights of the iron-based alloy (2605S-2); however, the error band obscured the statistical significance of the trend.

The two likely causes of the anisotropic wetting were 1) the surface topography and 2) a variation in the material properties across the ribbon width. The unidirectional nature of wetting in the immersion procedure causes the meniscus height measurement to be potentially sensitive to the surface morphology. The striations or channels, depending upon their depth, will enhance wetting (*i.e.*, increase the meniscus height) if they run parallel to the wetting direction, or they will hinder the wetting process if perpendicular to the wetting direction. It appeared that the effect of surface topography was not a probable source of the wetting behavior described by the data in Table 4 because opposing trends were observed on the wheel and exposed surfaces, despite the surface striations having had the same orientation.

Experiments by other investigators provide evidence that the orientation-dependent meniscus heights were caused

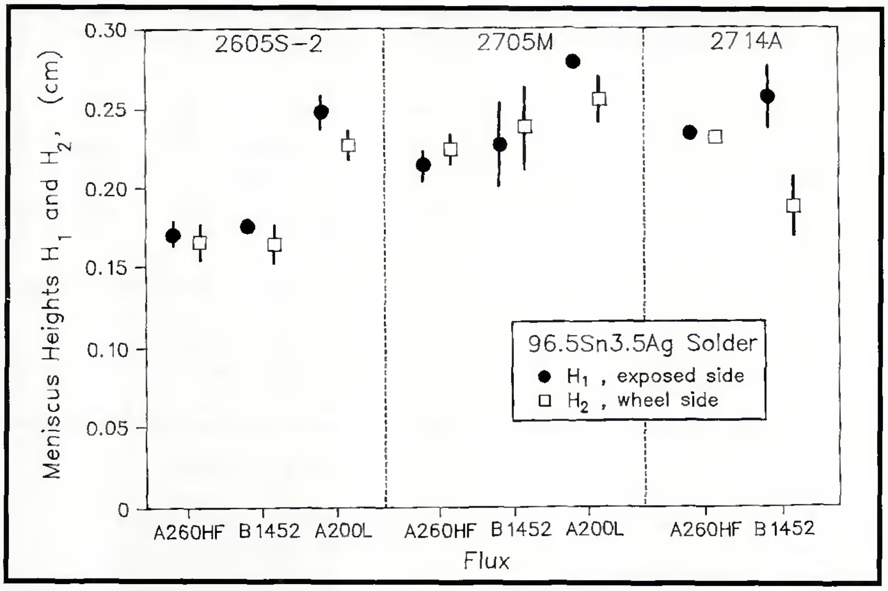

Fig. 7 — Meniscus heights on the wheel and exposed surfaces of the various metallic glass alloys, using 96.5Sn-3.5Ag solder and each of the flux candidates.

by variations in material properties across the ribbon width. Qualitative Auger depth profile analysis performed on 2705M and 2605S-2 samples did not show a significant variation in the large-scale chemical composition from the edge toward the center of the samples. Although not evaluated as part of this study, other investigators have observed variations of the more subtle short-range order (which includes both chemical and geometric atomic arrangements) across the ribbon width (Ref. 8). These variations can be caused by slight differences in the quenching rate across the ribbon geometry (Refs. 9, 10). Also, short-range structural changes have been detected between the wheel and exposed surfaces (Ref. 11).

In the case of the 2705M samples, wetting balance tests were performed for both orientations. The value of γ_{LF} was calculated to be 485 dyne/cm and 515 dyne/cm for the vertical and horizontal orientations, respectively. These values are well within experimental error and confirmed that the solder-flux interfacial tension was insensitive to sample orientation.

As noted earlier, all of the subsequent data in this report were taken from samples tested with the casting direction in the vertical orientation for procedural consistency.

Meniscus Heights and Tilt of the Coupon

The magnitude of the tilt angle caused by nonhomogeneous wetting was assessed from the experimental data. The meniscus heights of 96.5Sn-3.5Ag solder for each of the metallic glass alloys and fluxes are shown in Fig. 7. The values of H_1 and H_2 were most dissimilar for the 2714A when tested with the B1452 flux. Given a value of 2.54 cm for L_3, the tilt angle, δ, for this data set was computed to be 0.93 deg, a magnitude which is well within the normal experimental error of sample alignment. In conclusion, the differences, if any, between the two meniscus heights formed on the metallic glass samples were not large enough to affect the wettability parameters in this study. The meniscus heights and associated values of δ for the 95Sn-5Sb solder alloy demonstrated similar variations.

Solderability Parameters

The wetting balance curves demonstrated varying degrees of negative meniscus weights which occur just after immersion. Data from the tests: 95Sn-5Sb, A260HF, 2705M; and 95Sn-5Sb, A260HF, 2714A appear in Fig. 8. A survey of this behavior clearly indicated that it was dependent upon all three factors: flux, solder, and substrate alloy. Most interesting was a distinguishable difference between the cobalt-based alloys, 2714A and 2705M. In fact, the 2714A material showed no negative meniscus at the start of testing, irrespective of the solder or flux. These observations illustrate the effect of Mo additions on the wetting behavior. The role of Mo on the speed with which wetting takes place may arise through differences in the atomic structure of the metallic glass alloy, or by indirect effects which the structure may have through oxide film formation or surface chemistry.

The values of the contact angles, $\theta_{c,1}$ and $\theta_{c,2}$ for the 95Sn-5Sb solder are shown in Fig. 9. The 2714A alloy was not tested with the inorganic acid flux. The midpoint of each bar is the average contact angle; the length of the bar is the scatter range as defined earlier. The contact angles were similar for a given metallic glass alloy when coated with either of the organic acid fluxes (A260HF and B1452). The two surfaces of each substrate foil showed similar contact angles except in the case when A200L was used on 2605S-2. In this instance, a meniscus height difference of 0.03 cm caused the mean contact angles to differ by 6 deg. Overall, the values of the contact angles tended to be slightly lower on the cobalt-based ribbons than on the iron-based material. The A200L flux caused a slight decrease in the contact angles on the 2605S-2 alloy. However, a large drop in the mean contact angle to values of between 25 and 27 deg was recorded on the cobalt-based 2705M material with the A200L flux when compared to tests that used the organic acid fluxes.

Qualitatively, the data in Fig. 9 show a number of interesting points. First, the magnitude of the contact angles were compared to those of the more traditional solder-substrate systems. For example, the contact angle of 60Sn-40Pb solder on chemically etched oxygen-free, high-conductivity copper (OFHC) using the flux A260HF is 33 ±5 deg (Ref. 12). Using a mildly activated, rosin-based (RMA) flux, the value drops to 23 ±5 deg. 60Sn-40Pb solder on electropolished 29Ni-17Co-bal Fe alloy exhibits contact angles of 37 ±2 deg and 30 ±5 deg with A260HF and B1452, respectively (Ref. 3). The examples cited here represent "very good" to "excellent" wetting. The contact angle values for the metallic glass alloys (Fig. 9) are "fair" to "good." These results are interesting given that the substrate compositions contain cobalt, iron, nickel, and silicon. Typical crystalline materials which contain these elements form tenacious surface oxides that prevent solder wetting unless very aggressive cleaning procedures (such as chemical stripping or electropolishing) are performed on the material prior to solder coating. A second observation arising from Fig. 9 is that the A200L flux caused lower contact angles than did the organic acid fluxes. This trend suggests that the corrosive A200L flux more effectively increases the value of γ_{SF} or decreases the value of γ_{LF}, or both, when compared to the less corrosive, organic acid fluxes. The role of γ_{LF} will be further discussed later in the text. Moreover, the decrease was greater with the 95Sn-5Sb solder on the cobalt-based metallic glass (2705M) than on the iron-based metallic glass (2605S-2); illustrat-

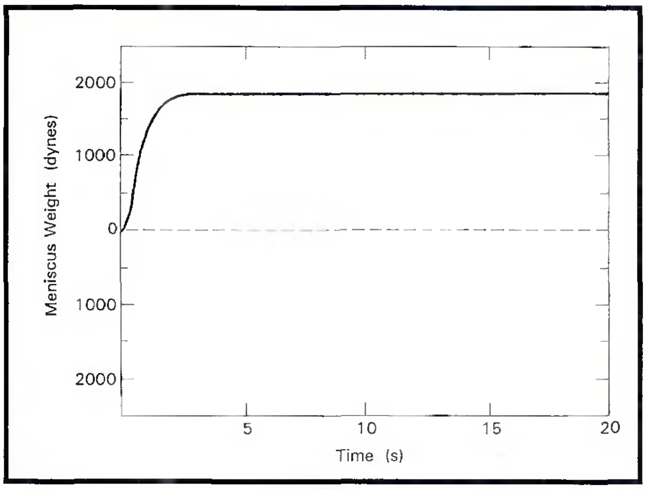

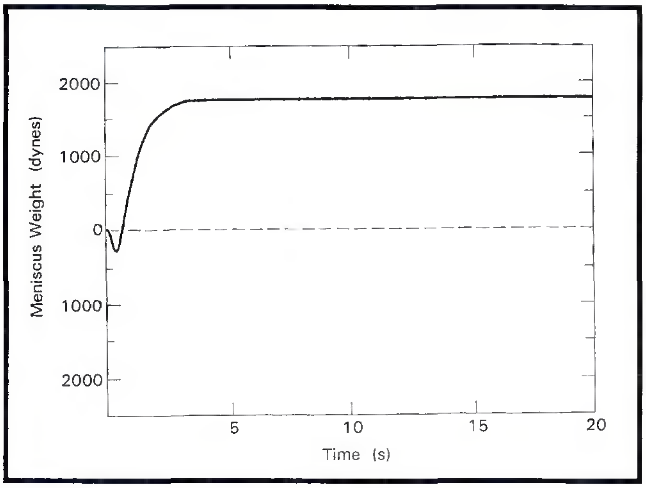

A **B**

Fig. 8 — Wetting curves using 95Sn-5Sb solder and A260HF flux. A — 2714A metallic glass; B — 2705M metallic glass.

ing the synergistic role between the substrate and flux chemistries on the wetting behavior.

The contact angle data for the 96.5Sn-3.5Ag solder are displayed in Fig. 10. The only significant difference between the contact angle values of the wheel and exposed ribbon surfaces was observed when B1452 flux was used on the 2714A metallic glass substrate. Use of A200L and 96.5Sn-3.5Ag solder on the iron-based substrate (2605S-2) caused a dramatic decrease in the contact angle when compared to tests with the organic acid fluxes. Conversely, only a very small improvement in $\theta_{c,1}$ and $\theta_{c,2}$ was observed with A200L on the 2705M material. When compared to the data in Fig. 9 for the 95Sn-5Sb solder and these two substrates, it is clear that the type of solder was a key factor in the apparent activity of the A200L flux to promote wetting.

A comparison can be made between the contact angles measured for the 96.5Sn-3.5Ag and 95Sn-5Sb solders. Other than the wetting behavior associated with the A200L flux as described above, the contact angle values were similar between the two solders with use of the two organic acid fluxes.

Neither of the two solder alloys demonstrated any obvious trends in the scatter range which accompanied the mean values of $\theta_{c,1}$ and $\theta_{c,2}$ as a function of either the flux or the metallic glass alloy.

In conclusion, the data in Figs. 9 and 10 demonstrate that the cobalt-based alloys showed slightly lower values of $\theta_{c,1}$ and $\theta_{c,2}$ than did the iron-based metallic glass for each of the solder-flux combinations. The minor composition variations between the two cobalt-based metallic glass alloys did not cause a significant difference in the values of the contact angles when the organic acid fluxes were used. In only two instances was an appreciable difference in the contact angles observed between the wheel and exposed surfaces of the foils: A200L, 2605S-2 alloy, with 95Sn-5Sb solder and B1452, 2714A ribbon, with 96.5Sn-3.5Ag solder. However, in neither case would the resulting sample tilt cause a

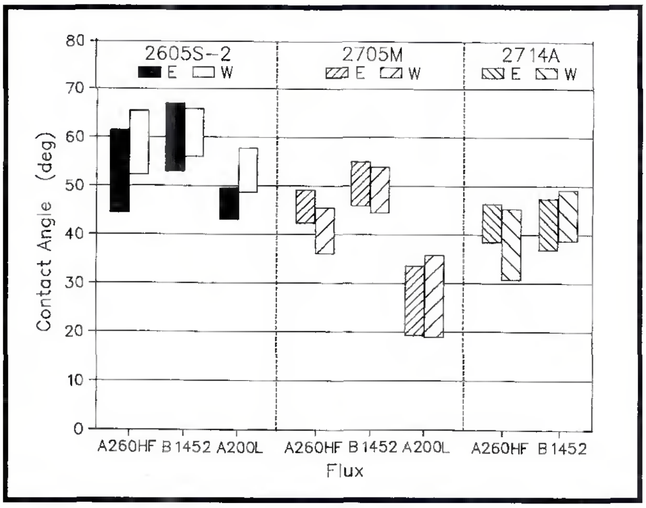

Fig. 9 — Contact angle values of 95Sn-5Sb solder on the various metallic glass substrates, using each of the candidate fluxes. "E" denotes the exposed surface and "W," the wheel surface.

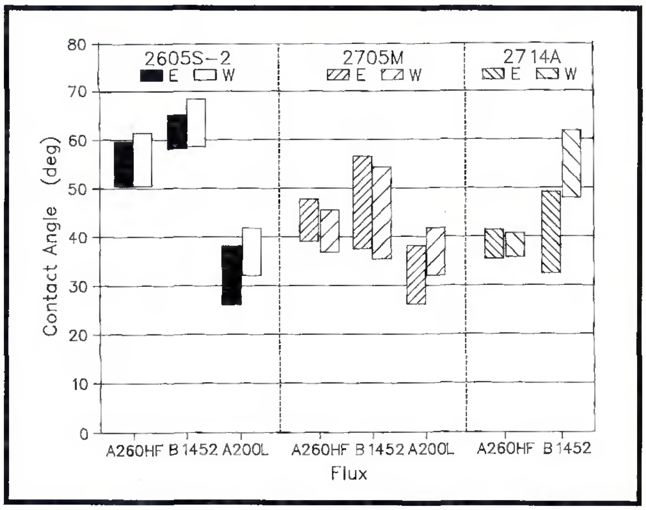

Fig. 10 — Contact angle values of 96.5Sn-3.5Ag solder on the various metallic glass substrates, using each of the candidate fluxes. "E" denotes the exposed surface and "W," the wheel surface.

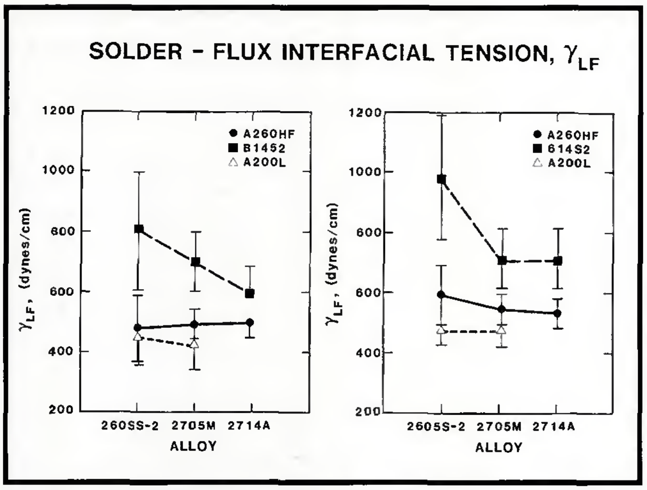

Fig. 11 — Solder-flux interfacial tension for each of the solder-flux-substrate systems investigated in this study.

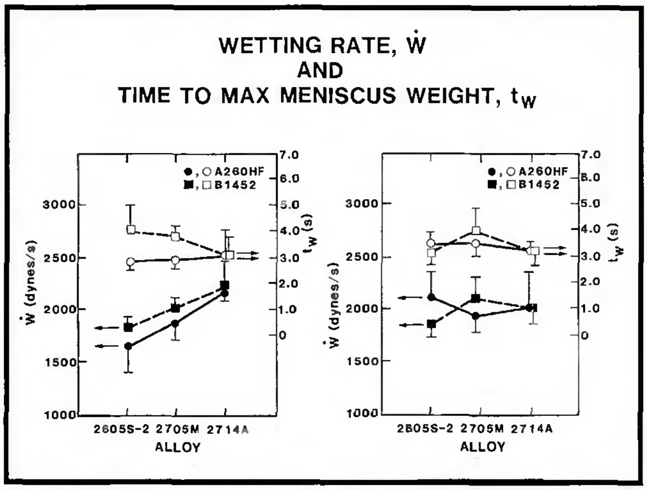

Fig. 12 — Wetting rate (closed symbols) and wetting time (open symbols) data for each of the solder-flux-substrate systems except those tested with the inorganic acid flux, A200L.

significant error in the measurements. Use of the A200L flux resulted in contact angles which depended explicitly upon the solder and metallic glass alloy; however, the general trend was toward lower contact angles when compared with use of the organic acid fluxes.

The solder-flux interfacial tensions (Fig. 11) had a significant impact on the contact angle values of each of the solder-substrate-flux systems when θ_c and γ_{LF} were analyzed through Young's equation — Fig. 2. Overall, the values of γ_{LF} were slightly higher with the 96.5Sn-3.5Ag solder than with 95Sn-5Sb; the likely cause being the presence of Ag in the former alloy which would tend to raise the solder's surface tension (Ref. 13). The B1452 flux caused significantly higher values of γ_{LF} for all of the solder alloy/metallic glass ribbon combinations and a larger scatter band when both solder alloys were used on the iron-based metallic glass substrate. The lowest values of the solder-flux interfacial tension were observed with the A200L flux which clearly contributed to the smaller contact angle values associated with this flux (Figs. 9, 10).

The data in Fig. 11 for the B1452 flux indicate that the solder-flux interfacial tension varies as a function of the metallic glass substrates. The variation was most pronounced between the iron-based 2605S-2 substrate and the two cobalt-based substrate with the 96.5Sn-3.5Ag solder. In the case of the 95Sn-5Sb solder, the values of γ_{LF} were again largest with the 2605S-2 substrate and declined in the order of 2705M and 2714A; however, the spread in the values obscures the statistical significance of the trend. The variation of γ_{LF} between the different metallic glass substrates signifies that reaction by-products created from the substrate surface (particularly for the iron-based alloy) by the activity of B1452 flux, had a minor influence on the solder-flux interfacial tension. Similar behavior was reported by Vianco, *et al.* (Ref. 3), in a wettability analysis of 60Sn-40Pb solder on bare 29Ni-17Co-bal Fe alloy, and was also observed in the re-analysis of data for 63Sn-37Pb on copper as function of flux activity (Ref. 4). Therefore, although the solder and flux compositions were the principal factors which determined the solder-flux interfacial tension, corrosion products generated by a particular flux (B1452) and substrate combination had a small, yet recognized effect on the value of γ_{LF}.

Table 5 — Qualitative Assessment of the Solder Films on the Metallic Glass Substrates

Flux	2605S-2 E	2605S-2 W	2705M E	2705M W	2714A E	2714A W
			95Sn 5Sb			
A260HF	Good	Good	Excellent	Excellent	Poor	V. Good
B 1452	Poor	Good	Excellent	Excellent	Poor	Poor
A200L	Dewetting	Dewetting	Dewetting	Dewetting	—	—
			96.5Sn 3.5Ag			
A260HF	V. Good	V. Good	Excellent	Excellent	Good	Excellent
B 1452	Good	Excellent	Excellent	Excellent	Good	Excellent
A200L	Dewetting	Dewetting	Dewetting	Dewetting	—	—

The wetting rate and wetting time data were also determined from the wetting curves. As noted earlier, these parameters include the combined behavior of both surfaces of the ribbon so that it is not possible to distinguish the wetting performance of each of the individual sample faces. The wetting rate, $\dot{W}$, was calculated from the positive slope of the wetting curve as depicted by the schematic diagram in Fig. 5. The wetting time, t_W, was determined as the elapse time required for $\dot{W}$ to attain its equilibrium value. The mean values of $\dot{W}$ and t_W for each of the solders, fluxes, and substrates are shown in Fig. 12. The error term represents one standard deviation. Only the organic acid fluxes were analyzed. First, the results of the 95Sn-5Sb solder will be reviewed. The B1452 and A260HF fluxes caused relative increases in the wetting rates in the order 2605S-2, 2705M, and 2714A; the variation was statistically significant only between the 2605S-2 and 2714A data. The 95Sn-5Sb solder displayed a significant difference in t_W between the two fluxes when tested with the 2605S-2 and 2705M substrates. The difference disappeared with 2714A. The larger mean wetting time values associated with B1452 and the 2605S-2 and 2705M substrates, when compared to the same flux and 2714A, reflect a combination of slower wetting rates and the presence of a negative meniscus at the start of the wetting curves.

The A260HF flux caused similar wetting times for all three metallic glasses, in spite of the observed wetting rate trend. In fact, the absence of a negative meniscus and a fast wetting rate which characterized the 2714A substrate material were expected to cause a significantly lower t_W for this particular substrate. This behavior was not observed because a

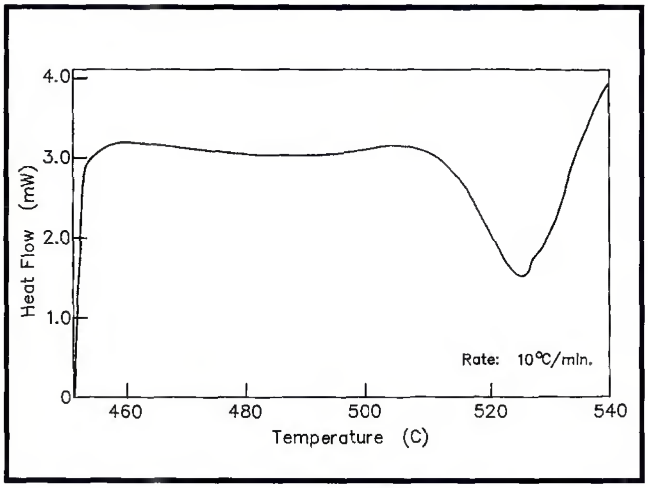

A

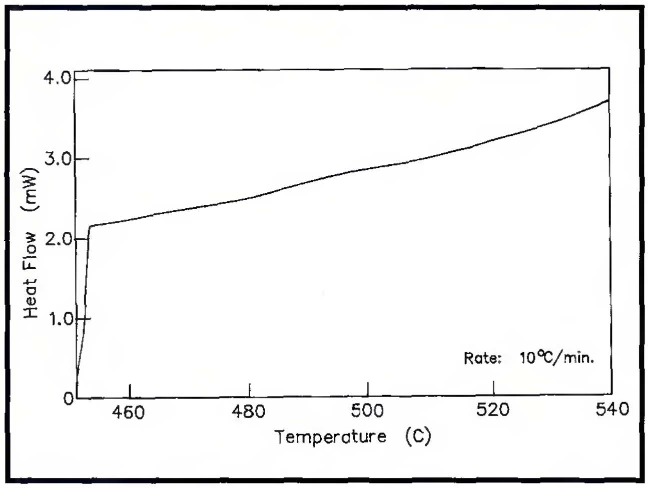

B

Fig. 13 — Differential scanning calorimetry (DSC) curves of the 2705M metallic glass. A — The as-received condition; B — after annealing at 550°C for 120 min.

longer elapsed time was required to reach the larger meniscus weights associated with the 2714A substrate.

The wetting rate data for the 96.5Sn-3.5Ag solder exhibited no significant trend as a function of metallic glass alloy, for any particular flux or as a function of flux per a given substrate. A similar trend was observed with the t_W data, as well. No particular property of the wetting curves was singularly responsible for the observed behavior. As with the 95Sn-5Sb solder, the decrease in t_W expected by an absence of the negative meniscus of the 2714A alloy, when compared to the other substrates, was generally negated by the added time necessary to reach W.

In summary, the time-dependent wetting data observed with use of the 96.5Sn-3.5Ag solder were not significantly different amongst the matrix of organic acid fluxes and substrate alloys tested with this solder. For the 95Sn-5Sb solder, the trend of increasing wetting rate in the order of 2605S-2, 2705M, and 2714A for either of the organic acid fluxes was obscured somewhat by the variability in the data. However, the values of t_W were significantly different between the two fluxes as well as the iron-based and one of the cobalt-based metallic glass substrates. This result indicates that the time-dependent wetting parameters were more sensitive to the substrate and flux with the 95Sn-5Sb solder than with the 96.5Sn-3.5Ag solder. This is contrary to the contact angle trends, which generally showed little difference between the two solder alloys, and illustrates the fact that the kinetic processes associated with solder wetting (as represented by W and t_W) do not necessarily reflect the equilibrium behavior (as represented by $\theta_{c,1}$ and γ_{LF}); the converse being likewise true.

Solder Film Evaluation

Accompanying the quantitative analysis of the wetting performance were qualitative observations of the solder films remaining on the coupons after their withdrawal from the solder pot. The appearance of the solidified solder films provided a measure of the wetting performance, which is critical for the complete evaluation of any solder-substrate-flux system. Shown in Table 5 is an assessment of the quality of the solder films remaining on the surfaces of samples used in the wetting balance tests. The solder films' topography was found to be sensitive to the withdrawal rate of the coupons; therefore, the wetting balance tests were used since they provided a repeatable withdrawal rate of 1.3 cm/s. The solder coatings were described as: "excellent" (complete, uniformly thick film), "very (v.) good," "good" (isolated regions of dewetting amounting to 10% of the immersed area), "poor" (dewetting over 25% of the immersed area), "dewetting" (100% of the immersed surface has dewetted) and "nonwetting" (the solder did not wet the surface as verified by the accompanying wetting balance curve). It is suggested by the data in Table 5 that the solder film appearance was dependent upon each of the parameters: solder, flux, substrate, and the particular ribbon face. Two trends were most apparent in the data. First, both of the organic acid fluxes caused excellent solder films on the surfaces of 2705M alloy, irrespective of the solder alloy. The second trend was that, in spite of producing the lowest contact angles amongst the fluxes, the flux, A200L, resulted in the poorest solder films. All of the samples coated with A200L showed complete dewetting on both ribbon surfaces. It is hypothesized that the dewetting resulted from the generation of nonwettable areas on the surface by the chemical activity of the flux (either caused by reaction by-products or the exposure of nonwettable areas from the subsurface region). Although the wettable areas supported the rising meniscus and its thicker layer of solder, those areas could not support the thin solder film remaining on the sample surface after withdrawal from the solder pot (Ref. 14). Wetting followed by dewetting upon sample withdrawal has been observed previously in solderability testing (Ref. 3).

An analysis was made of sample cross-sections using scanning electron microscopy and x-ray dot map techniques in order to investigate the solder-substrate interface for intermetallic compound formation and substrate dissolution. These studies were performed on the substrate-solder systems: 2705M, 96.5Sn-3.5Ag; 2705M, 95Sn-5Sb; 2605S-2, 96.5Sn-3.5Ag; and 2605S-2, 95Sn-5Sb. In all cases, a reaction layer was not observed at the interface, in spite of the 20 s immersion time, which can form a significant reaction layer at the solder-substrate interface of traditional crystalline materials (e.g., copper and nickel). Also, metal elements from the metallic glass substrate were not detected in the solder near the interface.

Effects of Structural Relaxation on Wettability

The goal of this series of experiments was to examine the role of the amorphous structure on wetting by the liquid solder. The data presented thus far sug-

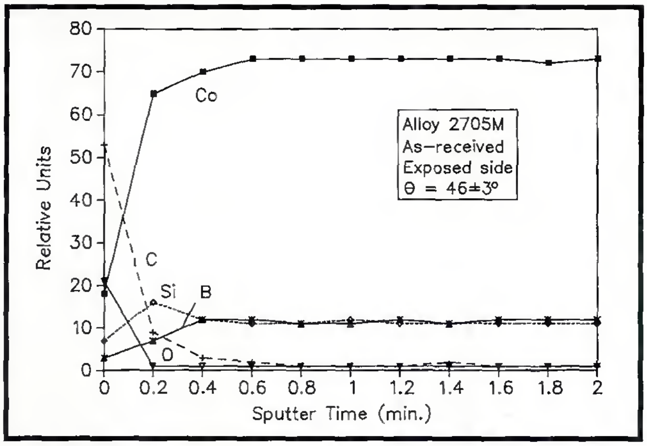

Fig. 14 — Auger depth profile spectrum of 2705M metallic glass samples in the as-received condition. The exposed surface was analyzed.

gest that the amorphous microstructure of the metallic glass alloys is responsible for the fair to good wetting demonstrated by the 95Sn-5Sb and 96.5Sn-3.5Ag solders either directly through the solder-substrate reaction as reflected by γ_{SL}, or indirectly by the nature of the surface chemistry or oxide layers (γ_{SF}). It must be emphasized that to hot solder coat iron-based *crystalline* substrates using the relatively mild organic acid fluxes is *impossible* without prior surface preparation (*e.g.*, chemical etching, electropolishing, mechanical abrasion, etc.) to remove the tenacious oxide layer (Ref. 3). A similar statement would also be applicable to cobalt-based materials. Moreover, the presence of easily oxidized constituents such as silicon would be expected to further deteriorate solderability. The next set of experiments will try to delineate the role of the metallic glass structure on solder wetting by changing the degree of randomness through structural relaxation.

The structural relaxation experiments were conducted with 95Sn-5Sb solder, the 2705M metallic glass alloy, and A260HF flux. The samples were heat treated in a 2 psia dry hydrogen atmosphere for 120 min at temperatures of 100°, 250°, 400° and 550°C (212°, 482°, 752° and 1022°F). Annealing was performed in dry hydrogen in order to prevent additional oxidation of the sample surfaces. The crystallization temperature of this material is 512 ±2°C as determined by differential scanning calorimetry (DSC), using a heating rate of 10°C/min (18°F/min). The annealing condition of 550°C and 120 min crystallized the ribbon structure; the other heat treatments resulted in only structural relaxation (*i.e.*, an increase in short range ordering) in the samples. Shown in Fig. 13A is the thermogram of the as-received material and in 13B, that of the specimen annealed at 550°C for 120 min. The exotherm in Fig. 13A indicates crystallization, but it is absent in Fig. 13B, signifying that the material was already crystallized by the heat treatment. Structural relaxation, which accompanied the other heat treatments, caused more subtle changes in the microstructure which were not easily distinguished on the DSC plots; the DSC curves for those samples appeared much like that of the as-received sample — Fig. 13A.

Shown in Table 6 are the contact angles, wetting rate, and wetting time data for the annealed 2705M samples. The contact angles of the coupons annealed at 100° and 250°C did not change appreciably from values of the as-received substrates. However, the wetting rates declined by approximately 10% from the as-received value; the wetting time, t_W, did not demonstrate a similar trend. Annealing at 400° and 550°C caused nonwetting by the solder with contact angles approaching 180 deg. The wetting behavior presented in Table 6 clearly indicated that the good wettability of the as-received metallic glass deteriorated when the samples were heat treated.

An Auger depth profile spectrum of the as-received 2705M foil appears in Fig. 14. The spectrum of the exposed surfaces are presented; the wheel side had similar results in all cases. A significant amount of carbon, which is a by-product of the fabrication process, is retained at the surface. The spectra were unchanged (to within experimental error) for the ribbons annealed at 100°, 250°, 400° and 550°C. There was no evidence that an excessively thick oxide layer had grown on the surface as part of the heat treating process, or that constituent elements had migrated to the surface. Both of these phenomena were capable of deteriorating the wetting behavior. Hydride formation on the sample surface as a source of deteriorated wetting could not be substantiated by the authors' review of the scientific literature.

The effect of structural relaxation and crystallization on solder wettability is clearly established; however, a determination of the root cause(s) has yet to be made. The mechanism(s) responsible for the results illustrated in Table 6 can be either a direct result of the changing structure, or caused by other properties which are sensitive to the sample structure. These mechanisms are best understood when reference is made to Young's equation — Fig. 2. For example, the direct influence of the atomic structure may be present through the metallurgical reaction at the solder-substrate interface. This would be reflected by changes to the value of γ_{SL}. Assuming that γ_{SF} or γ_{LF} remain unchanged, then the higher contact angles after structural relaxation/crystallization would be caused by an increase to γ_{SL}.

A direct role by γ_{SF} on wetting (with the other surface tensions being equal) would require that $\gamma_{SF/amorphous} > \gamma_{SF/crystalline}$. Given that the amorphous structure is a metastable, higher energy configuration as compared to the crystalline structure (which is the reason for structural relaxation at elevated temperatures), a reasonable assumption is that the surface energy would likewise be higher in the metallic glass than for its crystalline counterpart. If the opposite relationship were true, that is, $\gamma_{SF/amorphous} < \gamma_{SF/crystalline}$, then the direct dependence on structural relaxation/crystallization shown by the wettability behavior in Table 6 would be determined solely by γ_{SL}.

An indirect role played by the metallic glass structure on the degree of solder

Table 6 — Solderability Parameters for 95Sn-5Sb on 2705M Metallic Glass as a Function of Thermal Annealing

Annealing Temperature (C)	θ_c Exposed (deg)	θ_c Wheel (deg)	Wetting Rate (dyne/s)	Wetting Time (s)
As-received	46 ± 3	41 ± 4	1910 ± 150	2.9 ± 0.3
100	42 ± 8	41 ± 8	1640 ± 120	3.6 ± 2.0
250	52 ± 7	42 ± 7	1710 ± 60	2.9 ± 0.2
400	<180	<180	—	—
550	180	180	—	—

wettability is through the post-anneal oxide formation on the sample surface. The oxide layer tends to decrease the value of γ_{SF}, hence its removal and subsequent increase in γ_{SF} improves solder wetting. Structural relaxation may have caused the formation of a slightly thicker oxide layer, the difference having gone undetected by the Auger analysis. The inability of the flux to remove the oxide would lead to the poorer wettability observed in the Table 6 data. This scenario would support the earlier presumption that poor solderability of crystalline alloys containing the elements iron, cobalt, molybdenum, or silicon was due to the tenacity of the native oxide layer formed on the surface.

Conclusions

1) Wettability has been evaluated for 95Sn-5Sb and 96.5Sn-3.5Ag solders on one iron-based and two cobalt-based metallic glasses, using two organic acid fluxes and an inorganic acid flux. No extensive surface preparation beyond a solvent degreasing treatment was performed on the substrates.

2) Mean contact angles were in the range of 25 to 60 deg, being somewhat higher for the iron-based substrates and towards the lower values of the range for the cobalt-based material.

3) The distinct morphologies on the two ribbon surfaces arising from the casting process were observed. Analytical expressions were derived to quantify the effects of nonsymmetric meniscus heights. The analysis demonstrated that the different wettabilities did not significantly affect the experimental measurements, nor the calculation of the contact angles.

4) The minor alloy differences between the two cobalt-based metallic glasses were not reflected in the contact angle data but did influence the wetting rate and wetting time results as well as the quality of the solder film remaining on the specimens.

5) Use of the inorganic flux produced the lowest contact angles, yet caused complete dewetting of the solder films for all samples, upon their withdrawal from the solder pot.

6) The wettability of the metallic glass substrates deteriorated after thermal annealing in an H_2 atmosphere. Excessive oxide formation from the furnace conditions or the migration of alloying elements within the samples were not observed using of Auger depth profile analysis. The formation of an undetectable oxide layer caused by the increased short range order (structural relaxation) or long range order (crystallization) in the annealed samples, or the direct role alloy structure through the character of solder-substrate interfacial reaction (γ_{SL}), were possible sources of the deteriorated wettability.

Acknowledgment

This work was performed at Sandia National Laboratories for the U.S. Dept. of Energy under contract DE-AC04-76DP00789.

References

1. Chen, H. 1980. Metallic glasses, *Rep. Prog. Phys.*, 43:353.

2. Davis, L., DeCristofaro, N., and Smith, C. 1980. Technology of metallic glasses, *Proc. Conf. on Metallic Glasses: Science and Technology.* Budapest, Hungary.

3. Vianco, P., Hosking, F., and Rejent, J. 1990. Solderability testing of Kovar with 60Sn-40Pb solder and organic fluxes. *Welding Journal*, 69:230-s.

4. Mayhew, A., and Monger, K. 1972. Solderability by meniscometry. *Proc. Inter. NEPCON IV*, p.53.

5. Singer, F. 1975. *Engineering Mechanics, Part I — Statics.* Harper and Row, New York, N.Y., pp.190–216.

6. Alpha is a registered trademark of Alpha Metals, Inc., Jersey City, N.J.

7. Blackstone is a registered trademark of Blackstone Corp., Jamestown, N.Y.

8. Cao, X., and Li, J. 1985. Reverse shear of shear bands and annealing embrittlement in amorphous alloy. *Acta Met.* 33:499.

9. Inoue, A., Chen, H., Krause, J., and Masumoto, T. 1984. The effects of quench rate and cold drawing on the structural relaxation and Young's modulus of an amorphous 77.5Pd-6Cu-16.5Si wire. *J. Non-Cryst. Solids.*, 61 and 62:949.

10. Chi, G., Chen, H., and Miller, C. 1978. The influence of quenching procedures on the kinetics of embrittlement in a 40Fe-40Ni-20B metallic glass. *J. Appl. Phys.*, 49:1715.

11. Leimkuhler, A., Pond, R., Green, R., and Moran, P. 1986. Structural homogeneity, crystallization, and embrittlement behavior of amorphous 81Fe-13.5B-3.5Si-2C. *J. Non-Cryst. Solids.*, 81:141.

12. Vianco, P., Hosking, F., and Frear, D. 1991. Lead-free solders for electronics applications: wetting analysis. Proc. 4th Elec. Mater. and Proc. Congress, ASM, Inter., Materials Park, Ohio, to be published.

13. Murr, L. 1975. *Interfacial Phenomena in Metals and Alloys*, Addison-Wesley, Reading, Mass., p.104.

14. Klein-Wassink, R. 1989, *Soldering in Electronics,* Electrochem. Pub., Ltd., Ayr, Scotland, U.K., pp. 73–76.